International Journal of Bioprinting

RESEARCH ARTICLE

3D-printed vascularized biofunctional scaffold for bone regeneration

Bojun Cao[1,2,3†], Jieming Lin[4†], Jia Tan[1,2,3†], Jiaxin Li[5], Zhaoyang Ran[1,2,3], Liang Deng[1,2,3], Yongqiang Hao[1,2,3*]

[1]Shanghai Key Laboratory of Orthopaedic Implants, Department of Orthopaedic Surgery, Shanghai Ninth People's Hospital, Shanghai Jiao Tong University School of Medicine, Shanghai, 200011, China

[2]Clinical and Translational Research Center for 3D Printing Technology, Shanghai Ninth People's Hospital, Shanghai Jiao Tong University School of Medicine, Shanghai, 200011, China

[3]Shanghai Engineering Research Center of Innovative Orthopaedic Instruments and Personalized Medicine, Shanghai Ninth People's Hospital, Shanghai Jiao Tong University School of Medicine, Shanghai, 200011, China

[4]Department of Orthopaedic Surgery, Renji Hospital, South Campus, Shanghai Jiao Tong University School of Medicine, Shanghai 201112, China

[5]Department of Orthopedics, The Second Affiliated Hospital of Harbin Medical University, Harbin, China

(This article belongs to the *Special Issue: Novel Methods, Processes, and Materials of Bioprinting*)

Abstract

3D-printed biofunctional scaffolds have promising applications in bone tissue regeneration. However, the development of bioinks with rapid internal vascularization capabilities and relatively sustained osteoinductive bioactivity is the primary technical challenge. In this work, we added rat platelet-rich plasma (PRP) to a methacrylated gelatin (GelMA)/methacrylated alginate (AlgMA) system, which was further modified by a nanoclay, laponite (Lap). We found that Lap was effective in retarding the release of multiple growth factors from the PRP-GelMA/AlgMA (PRP-GA) hydrogel and sustained the release for up to 2 weeks. Our *in vitro* studies showed that the PRP-GA@Lap hydrogel significantly promoted the proliferation, migration, and osteogenic differentiation of rat bone marrow mesenchymal stem cells, accelerated the formation of endothelial cell vascular patterns, and promoted macrophage M2 polarization. Furthermore, we printed hydrogel bioink with polycaprolactone (PCL) layer-by-layer to form active bone repair scaffolds and implanted them in subcutaneous and femoral condyle defects in rats. *In vivo* experiments showed that the PRP-GA@Lap/PCL scaffolds significantly promoted vascular inward growth and enhanced bone regeneration at the defect site. This work suggests that PRP-based 3D-bioprinted vascularized scaffolds will have great potential for clinical translation in the treatment of bone defects.

Keywords: 3D bioprinting; Vascularization; Platelet-rich plasma; Bone regeneration

1. Introduction

The repair and functional reconstruction of bone defects is a major issue in the field of orthopedics that needs to be addressed[1]. The "gold standard" in the treatment of bone defects is autologous bone grafting; nevertheless, their clinical application is hindered

†These authors contributed equally to this work.

***Corresponding author:**
Yongqiang Hao
(hyq_9hospital@hotmail.com)

Citation: Cao B, Lin J, Tan J, *et al*., 2023, 3D-printed vascularized biofunctional scaffold for bone regeneration. *Int J Bioprint,* 9(3): 702.
https://doi.org/10.18063/ijb.702

Received: December 3, 2022
Accepted: January 1, 2023
Published Online: March 8, 2023

by their limited sources and the need for surgical bone extraction, which may lead to complications such as nerve damage and infection[2,3]. Allogeneic bone grafts could cause adverse conditions such as immune reactions, failure to integrate with the host bone, and slow remodeling[4]. A 3D-bioprinted active scaffold can overcome these limitations and meet the needs of anatomical remodeling and functional repair of bone defects[5]. However, there are still many challenges in the application of 3D bioprinting technology for clinical bone defect repair, and the selection of bioinks with strong pro-vascularization ability and osteoinductive bioactivity is the first challenge that needs to be overcome[6].

Osteogenic inducing factors represented by bone morphogenetic protein 2 (BMP-2) and pro-angiogenic growth factors represented by vascular endothelial growth factor (VEGF) are expensive and physicochemically unstable, and could lead to complications such as ectopic ossification and tumorigenesis, limiting their application in bone tissue engineering[7-9]. Finding an alternative, effective and safe "activating factor" that can be incorporated into 3D-printed active bone repair scaffolds is important. Platelet-rich plasma (PRP) is a platelet concentrate obtained by centrifugation of whole blood from animals or humans, which, when activated, releases multiple growth factors[10,11]. The proportions of the various growth factors released by PRP match the normal proportions present in the body, allowing for optimal synergy of each growth factor[12].

During normal fracture healing, VEGF expression typically peaks on days 5–10 after limb injury, while BMP-2 expression continues to increase until day 21, suggesting the need for delivery systems that support the sustained release of growth factors for long period of time[13-16]. However, once PRP is activated, its multiple growth factors are all released in a short burst, which is detrimental to the repair of bone defects[17,18].

Methacrylated gelatin (GelMA) and methacrylated alginate (AlgMA) have good biocompatibility and can form a uniform and stable pore-like structure within the gel after light-curing crosslinking, and a mixture of the two has better printability and mechanical properties[11,19-21]. In addition, bioactive molecules can be encapsulated in GelMA/AlgMA (GA) hydrogels and released slowly by diffusion, thus prolonging their retention time in bone defect sites[22]. On the other hand, nanoclays, such as laponite (Lap), have emerged as a new class of biocompatible materials with strong drug loading capacity and have potential to become strength-enhancing additives[23,24]. Lap is a disk-shaped nanoparticle with a diameter of about 25 nm and a thickness of about 1 nm. The negatively charged surface and positively charged edges of Lap allow some positively charged growth factors such as VEGF to form strong electrostatic bonds with its surface, which can slow down the release of growth factors or other drugs[25]. The addition of Lap to hydrogels has also been shown to affect the mechanical properties of hydrogels[25]. In addition, Lap has been reported to modulate the immune microenvironment and promote bone defect repair through the release of Mg^{2+} and Si^{4+}[26,27]. These advantages inspired us to conclude that combining GA hydrogel, Lap nanoparticles, and PRP may be a promising combination strategy to achieve enhanced therapeutic effects of PRP by slowing the release of various growth factors.

In the present study, we constructed a PRP-GA@Lap composite bioink and demonstrated its function of sustained slow release of various growth factors. Moreover, we investigated its effects on the proliferation, migration, differentiation, and tubule formation of human umbilical vein endothelial cells (HUVECs) and rat bone marrow mesenchymal stem cells (BMSCs) by *in vitro* experiments and demonstrated that it promotes macrophage M2 polarization. This composite bioink was then printed layer-by-layer with polycaprolactone (PCL) to construct a bone repair scaffold using 3D printing technology. By implanting this scaffold subcutaneously and at the site of femoral condylar defects in rats, we found that this bioactive scaffold promotes rapid vascular growth into the scaffold and accelerates bone regeneration. This work demonstrates that PRP-based 3D-printed vascularized bioactive scaffolds have great potential for clinical translation in the treatment of bone defects.

2. Materials and methods

2.1. Primary culture of rat BMSCs

The bilateral femurs of 3-week-old male Sprague Dawley (SD) rats were quickly removed in a sterile environment, taking care to keep the marrow cavity closed. Then, ophthalmic scissors were used to cut the bone marrow cavity open at both ends on an ultraclean bench, and the bone marrow cavity was rinsed four to six times with α-MEM (Gibco) complete medium and placed in a 10-mL Petri dish using a sterile syringe. Then, the cells were placed in an incubator for 36–48 h of static culture. Nonadherent cells were carefully removed and the medium was replaced. When the cells grew to 85%–90% confluence, they were passaged, and the third or fourth passaged cells were used for subsequent experiments.

2.2. Preparation of PRP and hydrogel precursor solution

PRP was prepared from the whole blood of rats after systemic heparinization by two centrifugations to remove serum and red blood cells. GelMA and AlgMA were dissolved in

phosphate-buffered saline (PBS) in the ratio of 5:1 (w/w), mixed thoroughly and then filtered with a 0.22-μm membrane to prepare a 5% (w/v) GelMA and 1% (w/v) AlgMA (GA) mixed hydrogel precursor solution, and then PRP was added to construct the 20% PRP-GA (PRP-GA) hydrogel. 1% (w/v) laponite was added to obtain the PRP-GA@Lap hydrogel.

2.3. Printing of scaffolds

The scaffolds used in this experiment were printed with a 3D-Bioplotter (Bio-Architect; Regenovo, Hangzhou, China). Briefly, for hydrogel scaffold printing, the mixed bioink was loaded into the barrel with a needle diameter of 250 μm, and by adjusting the temperature controller of the syringe barrel between 12°C and 20°C to achieve stable filament deposition. The temperature of the print platform was set to approximately 4°C lower than the injection tube. The print speed was 10 mm/s, and the air compressor pressure was 0.16 MPa. The 3D bioprinting process was performed under an ultraviolet (UV) light source (405 nm, 0.5 W cm^{-2}) for rapid curing. Finally, the scaffolds were exposed to a 2% (w/v) $CaCl_2$ solution for 10 min to obtain a stable structure.

For the printing of bone repair scaffolds with PCL (Perstorp, Sweden) combined with hydrogel ink, the fiber spacing was set to 1.0 mm, the PCL particles were loaded into a nozzle with a 300-μm diameter barrel, the temperature was kept at 60°C, and the printing speed was 10 mm/s. The PCL and each group of hydrogel inks were then printed layer-by-layer to construct scaffolds with a diameter of 3 mm and a height of 4 mm.

2.4. Morphology and compressive modulus of each group of hydrogels

The samples of each group were sputtered with gold, and the cross-sections of the lyophilized hydrogels were observed by scanning electron microscopy (SEM, EVO MA10, Germany). C, Mg, and Si distribution in PRP-GA@Lap hydrogels was analyzed by energy dispersive spectroscopy (EDS). The pore size of the hydrogels was analyzed and measured using ImageJ software.

Cylindrical hydrogel holders were prepared for uniaxial compression tests. Stress–strain curves for the GA, PRP-GA, and PRP-GA@Lap hydrogels were obtained using a universal mechanical testing machine (Instron 5969, USA) at a crosshead speed of 5 mm/min. The compression modulus of each group of hydrogels is represented by the slope of the 10%–20% compression phase.

2.5. Swelling and degradation of the hydrogel scaffolds

For the swelling test of the hydrogel scaffolds, preweighed hydrogel scaffolds were immersed in PBS solution at 37°C. Thereafter, they were removed at set time intervals, the surface liquid was wiped off, and they were weighed until the weight remained constant, indicating the swelling was completed. The swelling ratio was calculated using the following equation:

$$\text{Swelling ratio}\,(\%) = \frac{W_t - W_0}{W_0} \times 100\%$$

where W_0 and W_t refer to the weight of the hydrogel scaffolds at the initial and set time points, respectively.

In the degradation test, the hydrogels were weighed, placed in PBS and incubated at 37°C. Samples were removed at each set time point, lyophilized and weighed (dry weight, W_t). W_0 represents the initial dry weight, and the degradation rate (DR) for each sample was calculated by using the following equation:

$$\text{DR}\,(\%) = \frac{W_0 - W_t}{W_0} \times 100\%$$

2.6. Growth factor release kinetics from the hydrogel scaffolds

The release of multiple growth factors from two groups of hydrogel scaffolds containing PRP was tested by enzyme-linked immunosorbent assays (ELISAs). Briefly, groups of hydrogels were added to 50-mL centrifuge tubes containing PBS and placed at 37°C. The supernatant in each group of test tubes was aspirated at each time point and stored in a −80°C refrigerator, and then an equal volume of fresh PBS solution was added to each test tube. At last, the concentrations of VEGF, platelet-derived growth factor (PDGF)-BB and transforming growth factor beta (TGF-β) were determined with ELISA kits according to the manufacturer's protocol.

2.7. Cell proliferation assay

Briefly, BMSCs were grown in 96-well plates at a density of 10,000 cells/well, and the proliferation assay was detected when the cells reached ~70% confluence. The Cell Counting Kit-8 (CCK-8) assay was performed according to the manufacturer's instructions as previously described[28,29].

2.8. Detection of osteogenic differentiation

Osteogenic differentiation of rat BMSCs was assessed by alkaline phosphatase (ALP) and Alizarin red staining. Groups of hydrogel solutions were spread at the bottom of 24-well plates, covering the bottom (~15 μL cm^{-2}), and then treated with light-curing and Ca^{2+} crosslinking. BMSCs were inoculated in the 24-well plates at a density of 5 × 10^4/well and cultured using α-MEM medium containing 10% fetal bovine serum. After the cell growth reached ~70% confluence, the BMSCs were cultured with osteogenic induction medium (supplemented with 0.1 μM dexamethasone [Sigma], 10 μM sodium β-glycerophosphate

[Sigma], and 50 μg/mL ascorbic acid [Sigma]). ALP staining was performed when the culture reached day 5. To detect the formation of calcified nodules, Alizarin red staining was carried out when the culture reached day 14.

2.9. Assay of macrophage polarization on each group of hydrogels

Groups of hydrogel solutions were added to 48-well culture plates to prepare hydrogel substrates, light-cured, crosslinked, and then crosslinked with Ca^{2+}. RAW264.7 cells were then grown on the hydrogel surface at a density of 4×10^3 for 3 days. Lipopolysaccharide (LPS) (100 ng/mL, 8 h) was then added to the culture medium (DMEM, Gibco) as an activator of M1 macrophages. Gene expression of M1-type markers and M2-type markers was determined by quantitative polymerase chain reaction (qPCR), followed by immunofluorescence analysis to detect arginase 1 (Arg1) and inducible nitric oxide synthase (iNOS) protein expression. Briefly, RAW264.7 cells were gently washed three times with appropriate amount of PBS, followed by fixation with 4% concentration of paraformaldehyde and finally permeabilization with 0.1% Triton X-100. Antibodies against Arg1 (Abcam) and iNOS (Abcam) were used for immunofluorescence staining. Nuclei were stained blue by DAPI and then observed under fluorescence microscopy.

2.10. Quantitative real-time PCR analysis

Briefly, total RNA from RAW264.7 was isolated with TRIzol reagent (Invitrogen). The primer sequences were: iNOS: forward 5′-(GTTCTCAGCCCAACAATACAAGA)-3′ and reverse 5′-(GTGGACGGGTCGATGTCAC)-3′; CCR7: forward 5′-(GAGGCTCAAGACCATGACGGA)-3′ and reverse 5′-(ATCCAGGACTTGGCTTCGCT)-3′; Arg1: forward 5′-(GGTGGCAGAGGTCCAGAAGAA)-3′ and reverse 5′-(CCCATGCAGATTCCCAGAGC)-3′; CD206: forward 5′-(CTCTGTTCAGCTATTGGACGC)-3′ and reverse 5′-(CGGAATTTCTGGGATTCAGCTTC)-3′. GAPDH was used as an internal control for expression normalization.

2.11. Western blot analysis

The antibodies involved in this study were utilized as follows: PCNA (Abcam), β-actin (Abcam) and cyclin D1 (Abcam). An ImageQuant LAS4000 imaging station (GE) was used to acquire images.

2.12. Subcutaneous implantation experiment in rats

After the rats were fully anesthetized, small incisions were made on both sides of their backs, and each group of bone repair scaffolds was implanted under the skin on both sides of the rats' backs. The scaffolds were removed at 4 weeks after surgery and the samples were sectioned and subsequently stained.

2.13. Hematoxylin–eosin staining and immunofluorescence staining

Each groups of bone repair scaffolds were fixed, embedded, and sectioned, followed by hematoxylin–eosin (HE) staining and picture acquisition with a Nikon microscope. Immunofluorescence staining was performance in accordance with the standard protocol described previously[29] with α-SMA (Abcam) or CD31 (Abcam) antibodies.

2.14. Construction of the rat femoral condyle defect model and implantation of a bone repair scaffold

The rat femoral condyle defect model was utilized to verify the *in vivo* bone repair capacity of each group of scaffolds. At approximately 8 weeks, male SD rats weighing approximately 300 g were chosen for establishing the femoral condyle defect model. Briefly, the femoral condyles are exposed through an incision in the distal femur of the rat. To avoid thermal necrosis, a cylindrical defect, which is 3 mm in diameter and 4 mm deep, was constructed using a relatively low speed electric drill precooled with iced PBS. After the fragmented bone was removed, the drill hole was flushed with saline, and the scaffold was implanted into the bone defect. The experiment was divided into four groups: GA/PCL group, PRP-GA/PCL group, PRP-GA@Lap/PCL group, and blank control group; animal tissue sampling was performed 1 month after surgery.

All protocols involving experimental animals were approved by the Animal Welfare Ethics Committee of the Ninth People's Hospital Affiliated to Shanghai Jiaotong University School of Medicine.

2.15. Radiographic evaluation

The effect of each group of scaffolds on the repair of bone defects was examined using a micro-CT system (SkyScan 1176, Bruker, Belgium). The specific scanning parameters were as follows: 18 μm resolution, 1 mm aluminum filter, 90 kV voltage, and 250 μA current. Three-dimensional reconstruction was performed using simulation software (CTVol). The ratio of bone volume to total tissue volume (BV/TV) and bone mineral density (BMD) was quantified.

2.16. Statistical analysis

Results are expressed as the mean ± standard deviation (SD), and statistical analysis was performed using GraphPad Prism 8.0. One-way analysis of variance (ANOVA) followed by Tukey's multiple comparison tests was applied for comparisons between multiple groups, and Student's *t*-tests were applied for comparing differences between two groups. Kruskal–Wallis tests were utilized to analyze the nonparametric data. A value of $P < 0.05$ was considered statistically significant.

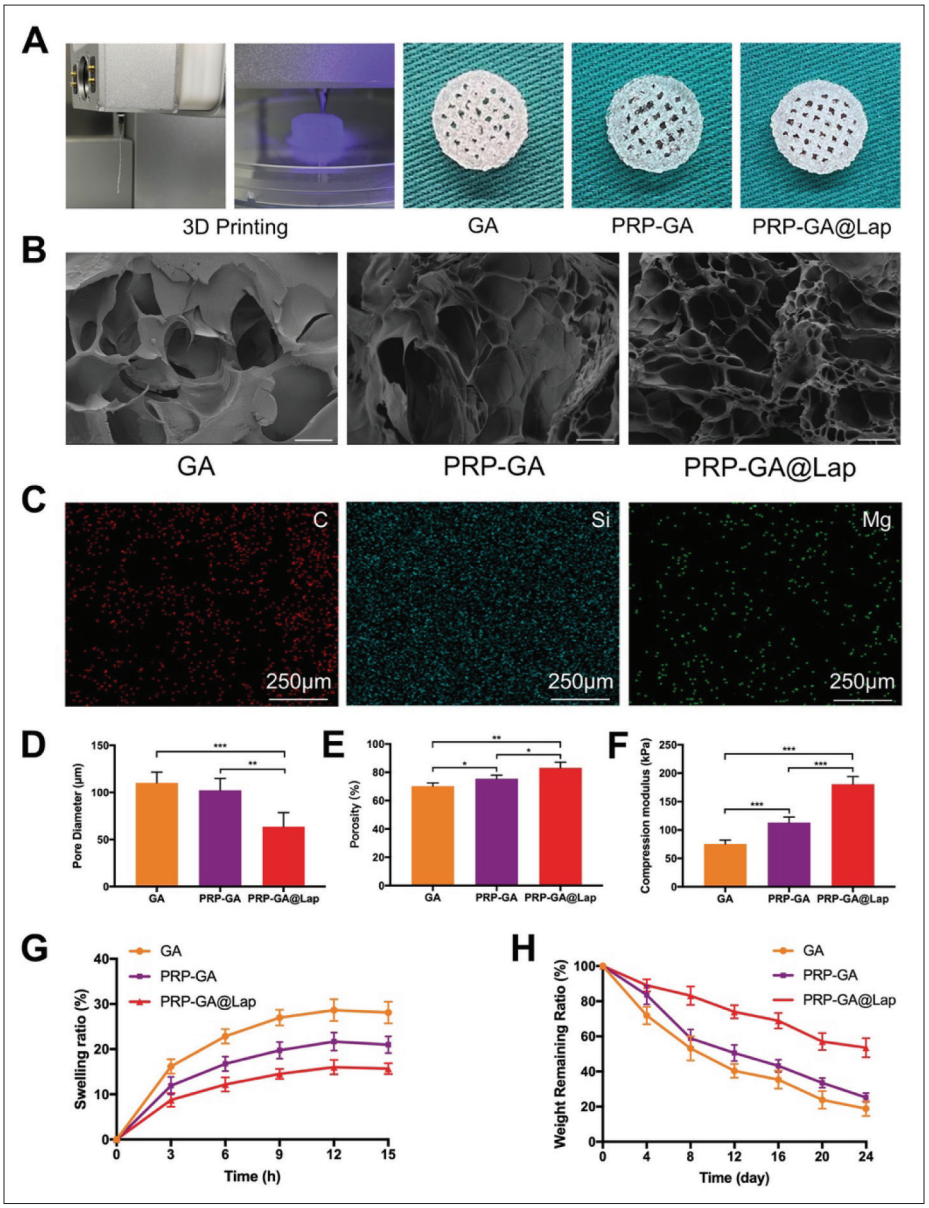

Figure 1. Characterization of each group of hydrogels. (A) 3D printing of each group of hydrogel scaffolds and representative images. (B) Representative SEM images of each group of hydrogels. (C) X-ray energy dispersive spectral mapping images of PRP-GA@Lap hydrogel: C (red), Si (cyan) and Mg (green). (D) Pore size of each group of hydrogels (n = 6/group). (E) Porosity size of each group of hydrogels (n = 4/group). (F) Compressive modulus of each group of hydrogels (n = 4/group). (G, H) The swelling properties and degradation curves of each group of hydrogels (n = 3/group). All experiments were replicated three times, $^{*}P < 0.05$, $^{**}P < 0.01$, and $^{***}P < 0.001$.

3. Results

3.1. Preparation and characterization of the hydrogels

We successfully prepared PRP from rats and then mixed it with GA and Lap in appropriate proportions to make GA, PRP-GA, and PRP-GA@Lap hydrogel precursor solutions, respectively, and then prepared each group of hydrogel scaffolds by 3D bioprinting (Figure 1A). We observed that PRP-GA@Lap hydrogels had better printing accuracy.

The internal morphology of the lyophilized GA, PRP-GA, and PRP-GA@Lap hydrogels was examined by SEM. The SEM images of all hydrogels show interconnected porous microstructures, as shown in Figure 1B. We found that PRP-GA@Lap hydrogels tended to have a reduced pore size and rougher pore walls but a higher porosity as compared with the GA and PRP-GA hydrogels (Figure 1D and E), which indicates the enhanced crosslinking of the gels by the addition of Lap.

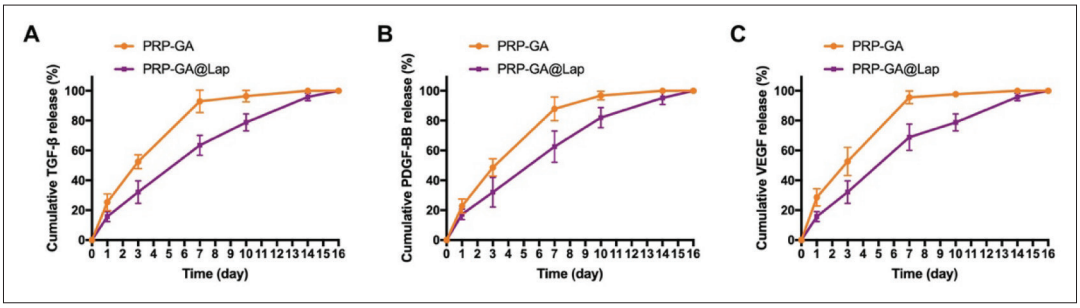

Figure 2. The growth factor release profiles of each group of hydrogels. (A–C) The release profiles of TGF-β, PDGF-BB, and VEGF (n = 3/group). All experiments were replicated three times.

In addition, the homogeneous distribution of Mg and Si^{4+} elements in the PRP-GA@Lap hydrogels was detected by EDS, which supports the homogeneous addition of Lap to the hydrogels (Figure 1C). The mechanical properties of each group of hydrogels were further revealed by compressive modulus assay (Figure 1F). The compressive moduli of GA, PRP-GA, and PRP-GA@Lap hydrogels were 75.55 ± 6.62 kPa, 113.00 ± 9.86 kPa, and 180.55 ± 13.44 kPa, respectively.

The degradation and swelling properties of hydrogels are critical for maintaining their stability and promoting tissue regeneration. As shown in the swelling curve (Figure 1G), PRP-GA@Lap reached a swelling equilibrium of 16.01 ± 1.61% after 12 h, with a significantly lower swelling rate than the GA and PRP-GA hydrogels groups. Similar to its swelling performance, PRP-GA@Lap exhibited a suitable degradation rate with a residual mass percentage of 53.57 ± 5.41% after 24 days and showed long-term stability in PBS (Figure 1H). The high crosslinking density of PRP-GA@Lap hydrogels resulted in a moderate degradation rate and a low swelling rate compared to the GA and PRP-GA hydrogels groups, and this stability facilitated tissue regeneration.

3.2. Release of growth factors from hydrogels

Activated PRP provides multiple growth factors that promote osteogenesis and neovascularization, and it is widely used in clinical practice to treat fractures, osteoarthritis, and difficult-to-heal wounds. However, the excessive initial burst release of growth factors by PRP limits its therapeutic effect. Previous studies reported that pure PRP gels released most of their growth factors rapidly within 2 days[30]. To determine whether PRP-GA and PRP-GA@Lap hydrogels have the ability to slow the release of growth factors, the release kinetics of PDGF, TGF-β and VEGF in the two groups of hydrogels were detected by ELISA. As shown in Figure 2A–C, the PRP-AlgMA@Lap hydrogel exhibited a sustained release of growth factors for about 2 weeks. Its slow-release effect was markedly better than that of the PRP-AlgMA hydrogel group.

3.3. Bioactivity of hydrogels

To assess the biocompatibility of each group of hydrogels, we observed the survival of rat BMSCs on the surface of the hydrogels using a live/dead staining assay. As shown in Figure 3A, the cells on the surface of the hydrogels of all groups grew well. Only a very small number of dead cells were observed, and there was no significant difference in the cell survival rate among the different gels. Using CCK-8 assay (Figure 3B), we found that the PRP-GA and PRP-GA@Lap groups significantly promoted the proliferation of BMSCs compared with the GA group, and the Western blot results showed that the expression of cyclin D1 and PCNA was significantly increased in the PRP-GA and PRP-GA@Lap groups compared with the GA group, which may be caused by growth factors released by PRP in the former to promote cell proliferation (Figure 3C–E). We also found that the leachate of the PRP-GA and PRP-GA@Lap hydrogels significantly promoted the migration of rat BMSCs by scratch assays (Figure 3F and G), which was further verified by Transwell assays (Figure 3H and I).

3.4. Effect on osteogenic differentiation of BMSCs

To investigate the effect of each group of hydrogels on the osteogenic differentiation of rat BMSCs, we grew BMSCs on the surface of each group of hydrogels separately and performed ALP staining after 5 days of incubation using osteogenic induction medium. The results demonstrated that the ability of the PRP-GA and PRP-GA@Lap hydrogels to promote the osteogenic differentiation of rat BMSCs was significantly higher than that of pure GA hydrogels (Figure 4A). Furthermore, we performed Alizarin red staining and quantitative analysis of the BMSCs in each group after 14 days of culture, and the results suggested that the PRP-GA@Lap group produced a large number of calcium nodules, significantly more than that in the other two groups (Figure 4B and C). These results demonstrated the potential osteogenesis-promoting properties of the PRP-GA@Lap hydrogel.

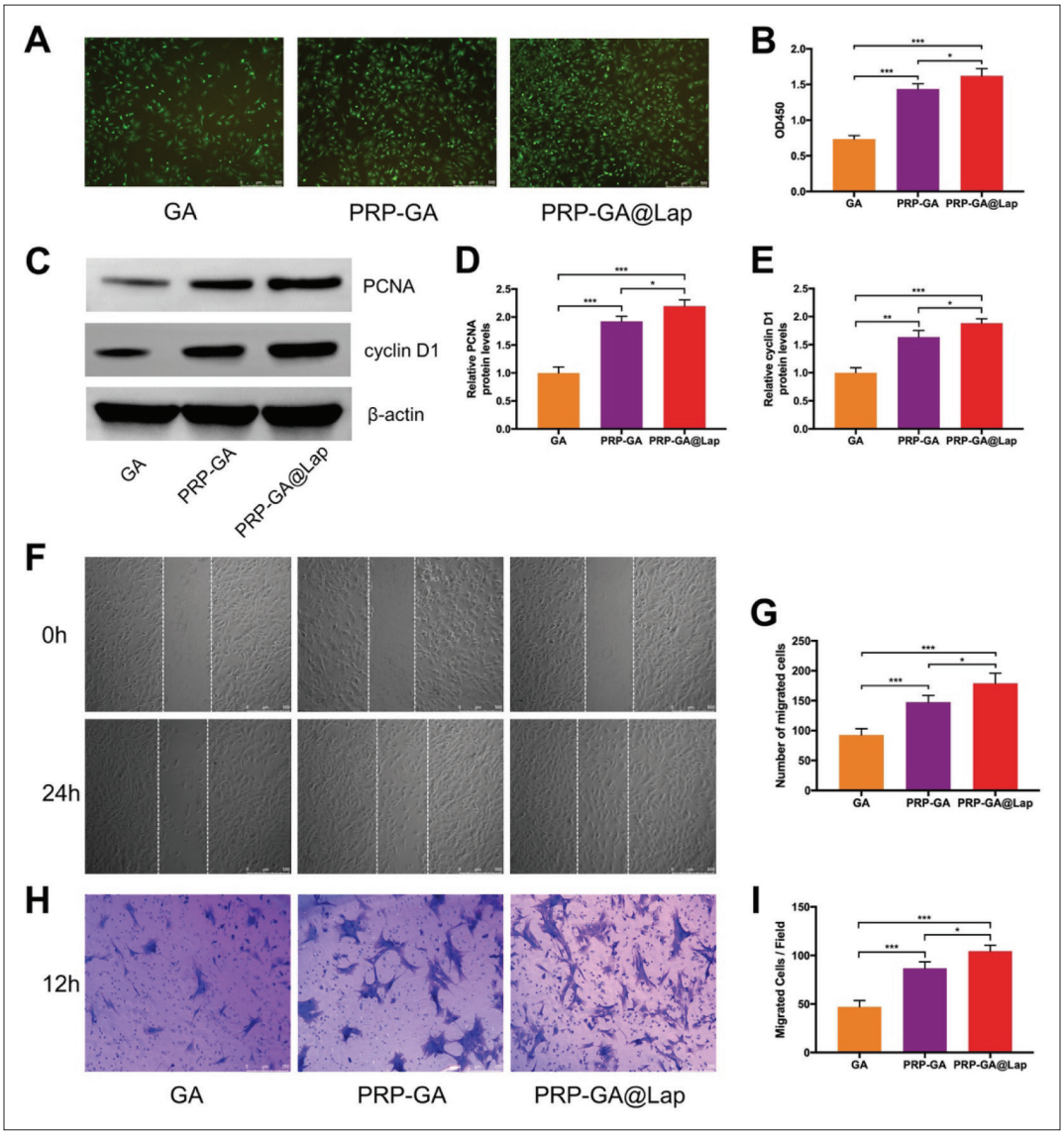

Figure 3. Assessment of cell viability of each group of hydrogels. (A) The *in vitro* cellular activity of each group of hydrogels was assessed using BMSC. (B) Detection of the effect of each group of hydrogels on BMSC proliferation by cell counting kit-8 (n = 3/group). (C–E) Expression of cyclin D1 and PCNA protein in each group of BMSC (n = 3/group). (F) The effect of each group of hydrogels on BMSC migration as determined by scratch-wound assay. The number of migrating cells was quantified and shown in (G); n = 4/group. (H) The effect of each group of hydrogels on BMSC migration as determined by Boyden chamber assay. The number of migrating cells was quantified and shown in (I); n = 3/group. All experiments were replicated three times. $^{*}P < 0.05$, $^{**}P < 0.01$, and $^{***}P < 0.001$.

3.5. Effects on the biological functions of HUVECs

We next examined the effect of the leaching solution of each hydrogel group on HUVEC proliferation using CCK-8, and the results suggested that PRP-GA and PRP-GA@Lap could significantly promote HUVEC proliferation (Figure 5A). The scratch assays and Transwell assays demonstrated that the PRP-AlgMA@Lap markedly promoted the migration of HUVECs compared with the other two groups (Figure 5B–E).

Furthermore, the effect of each group of hydrogels on HUVEC tubule generation *in vitro* was examined using a tubule formation assay. We directly grew HUVECs on the surface of the hydrogels of each group without using a dedicated matrix gel on the plates. After 6 h of incubation, we failed to observe significant tubule generation in the pure GA hydrogel group, while the PRP-GA@Lap group showed significant tubulogenesis, and the number and area occupied by the tubules were significantly higher than

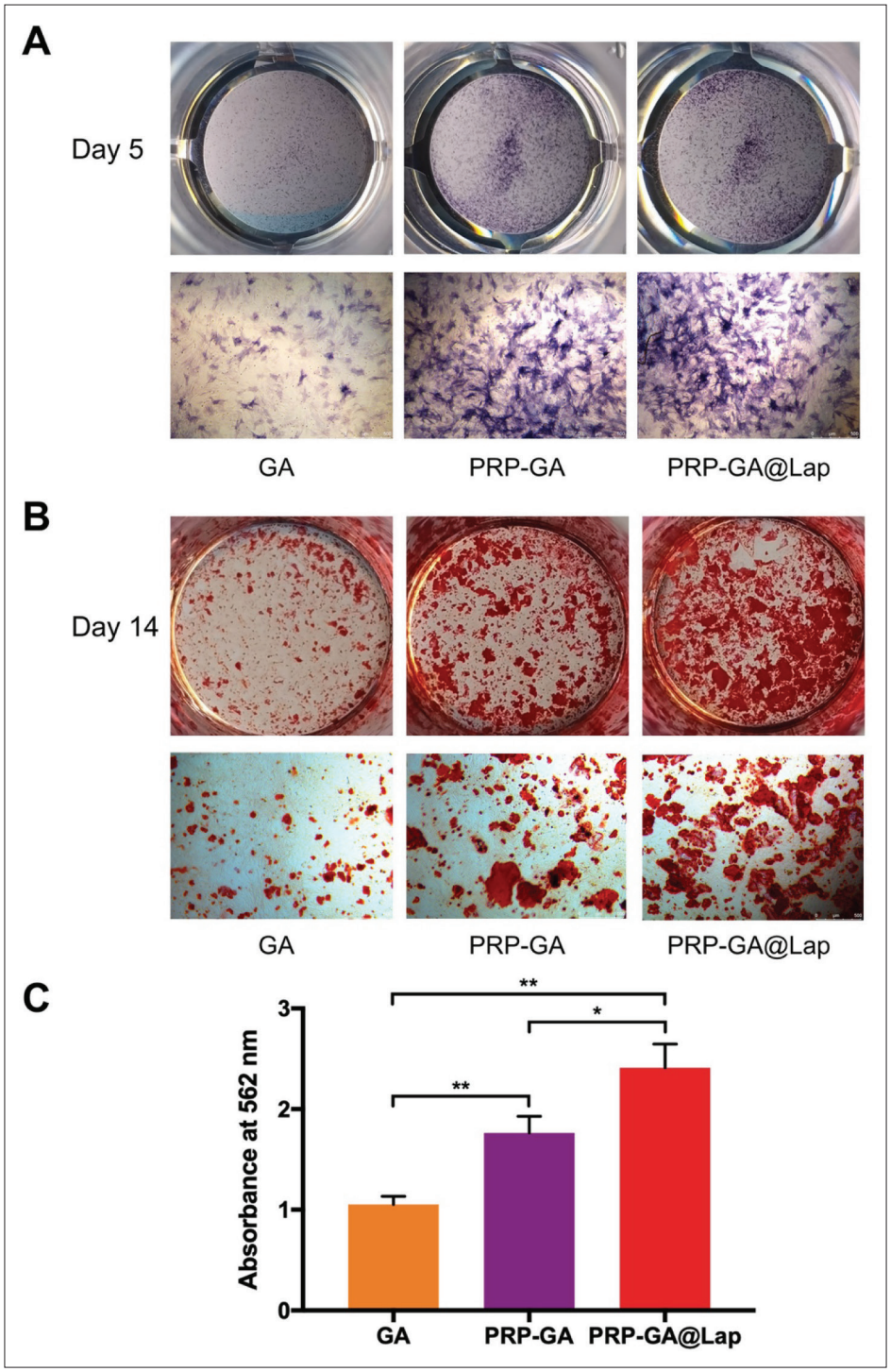

Figure 4. Effect of each group of hydrogels on osteogenic differentiation of BMSC. (A) ALP staining after 5 days of culture. (B) Alizarin red staining after 14 days of culture on each group of hydrogels. (C) Quantitative analysis of Alizarin red S staining (n = 3/group). All experiments were replicated three times. *$P < 0.05$ and **$P < 0.01$.

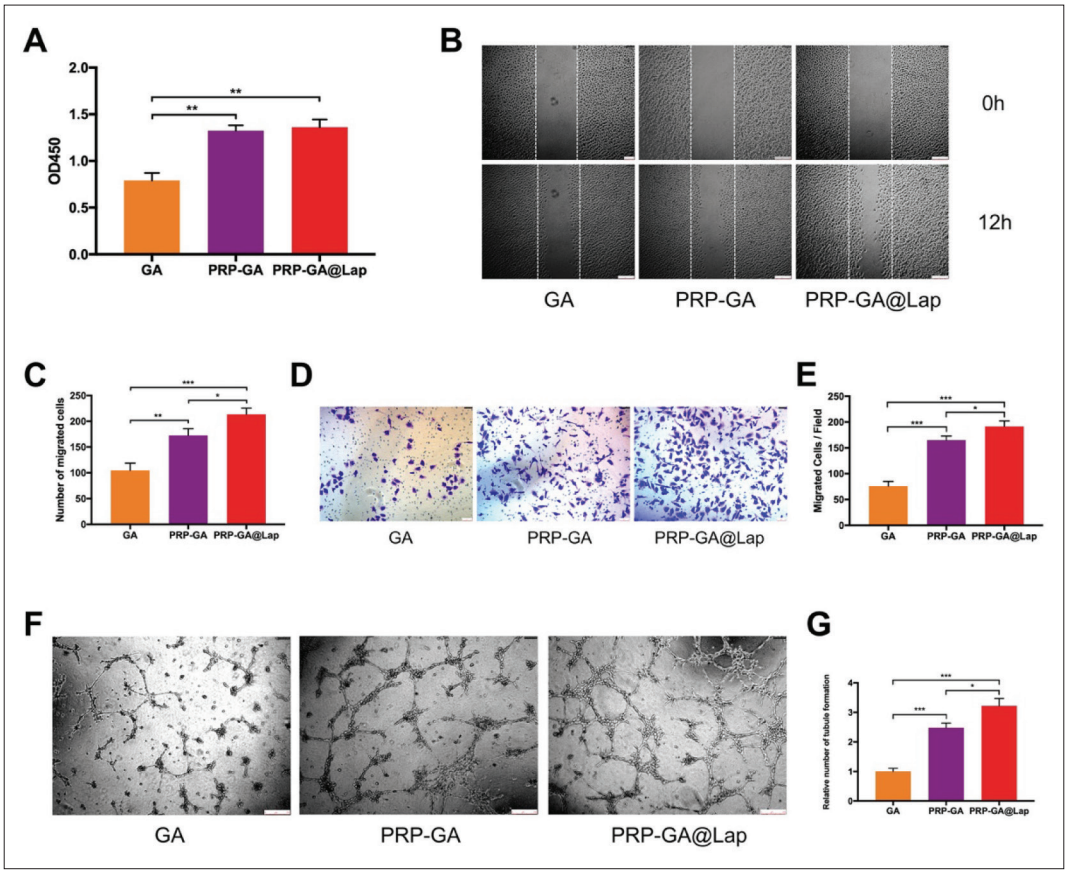

Figure 5. Effect of hydrogels on HUVEC proliferation, migration, and tubule formation. (A) Effect on the proliferation of HUVEC (n = 3/group). (B) The effect of each group of hydrogels on HUVEC migration as determined by scratch-wound assay. The number of migrating cells was quantified and shown in (C); n = 4/group. (D) The effect of each group of hydrogels on HUVEC migration as determined by Boyden chamber assay. The number of migrating cells was quantified and shown in (E); n = 3/group. (F) Effect on HUVEC tubule formation. (G) Relative number of tubule formation (n = 3/group). All experiments were replicated three times. *$P < 0.05$, **$P < 0.01$, and ***$P < 0.001$.

those in the PRP-GA group (Figure 5F and G). These results demonstrated the potential pro-angiogenic properties of the PRP-GA@Lap hydrogel.

3.6. Effect of hydrogels on macrophage polarization *in vitro*

We cultured RAW264.7 cells on each group of hydrogels to determine their effect on macrophage polarization. The qPCR results showed that the expression of iNOS and CCR7 (M1 marker) genes was decreased in cells cultured on PRP-GA and PRP-GA@Lap hydrogels compared to the pure GA group (Figure 6A and B), while the expression of Arg1 and CD206 (M2 marker) genes was increased (Figure 6C and D). In addition, the immunofluorescence staining results were consistent with the qPCR results (Figure 6E and F). These results demonstrated that both sets of hydrogels containing PRP could promote macrophage polarization to M2.

3.7. Vascularization effect of 3D-printed biofunctional scaffolds *in vivo*

We next used 3D-printed PCL and each group of hydrogel bioinks layer-by-layer to construct bone defect repair scaffolds (Figure 7A), and examined the compression modulus of pure PCL scaffolds and PRP-GA@Lap/PCL scaffolds (**Figure S1**). The scaffolds of each group were then implanted subcutaneously in the backs of rats to assess the vascularization effect of the scaffolds *in vivo* (Figure 7B). Four weeks after implantation, the number of vessel formation in the PRP-GA@Lap/PCL group was markedly higher than the other two groups as observed by HE staining (Figure 7C and D). Moreover, the vessels in the PRP-GA@Lap/PCL group were more mature, and in addition to the presence of erythrocyte perfusion (Figure 7C), we found that the PRP-GA@Lap/PCL group also had α-smooth muscle actin (α-SMA) and CD31

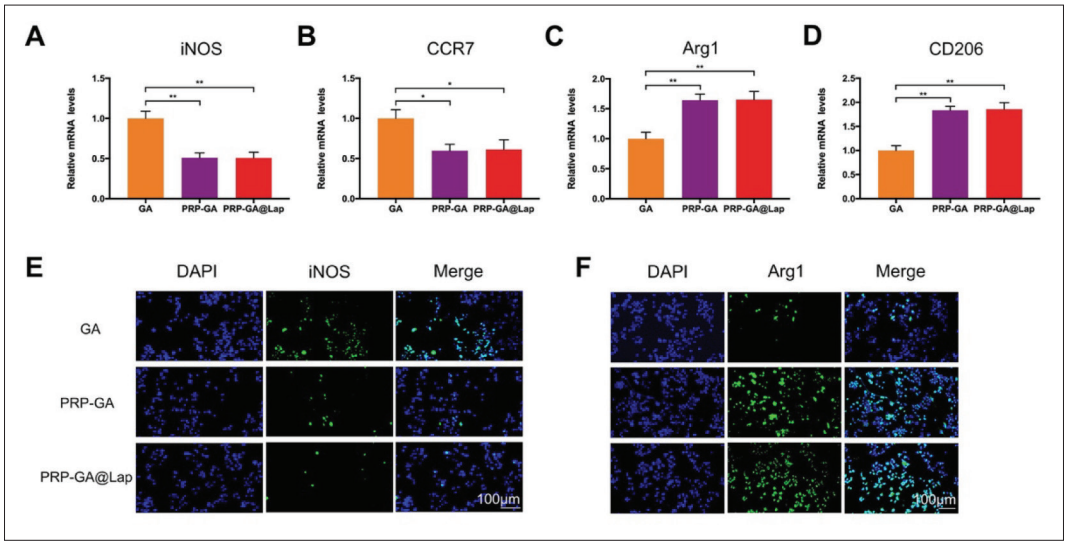

Figure 6. Effect of hydrogels on macrophage polarization *in vitro*. (A, B) Results of qPCR of M1-related gene expression (CCR7 and iNOS) (n = 3/group). (C, D) Results of qPCR of M2-related gene expression (CD206 and Arg1) (n = 3/group). (E) Immunofluorescence staining of iNOS in RAW264.7 cells cultured on each group of hydrogels. (F) Immunofluorescence staining of Arg1 in RAW264.7 cells cultured on each group of hydrogels. All experiments were replicated three times. $^{*}P < 0.05$ and $^{**}P < 0.01$.

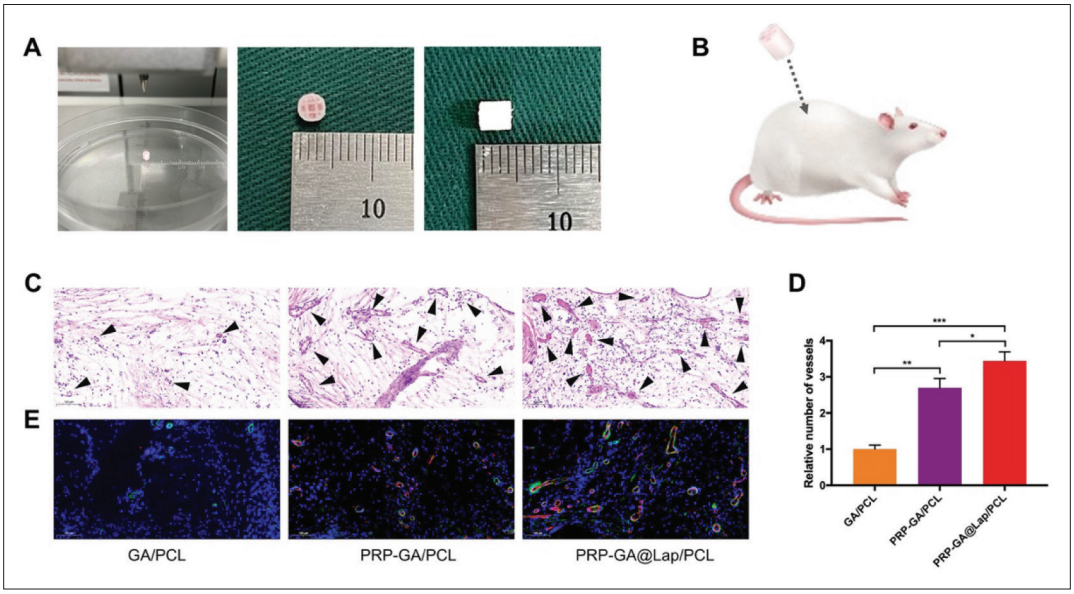

Figure 7. Vascularization effect of 3D-printed PRP-GA@Lap/PCL scaffolds *in vivo*. (A) Construction of each group of bone defect repair scaffolds by 3D printing. (B) Subcutaneous implantation in rats. (C) Representative HE-stained images of each group of scaffold sections. (D) Relative number of vessels in each group of scaffold sections (n = 4/group). (E) Immunofluorescence staining of nuclei (blue), α-SMA (green) and CD31 (red) in each group of scaffold sections. All experiments were replicated three times. $^{*}P < 0.05$, $^{**}P < 0.01$, and $^{***}P < 0.001$.

staining-positive vessel walls by immunofluorescence staining (Figure 7E).

3.8. Bone regeneration effects of 3D-printed biofunctional scaffolds *in vivo*

We next investigated the osteogenic function of each group of scaffolds by constructing a rat femoral defect model (Figure 8A). After 4 weeks of implantation, no infection or death occurred in any of the rats. X-ray examination revealed that the bone defect area in the PRP-GA/PCL group showed a higher density shadow than that in the blank control group and the GA/PCL group; however, it was significantly lower than that in the PRP-GA@Lap/PCL group (Figure 8B). Further micro-CT scanning and 3D image reconstruction revealed that new bone tissue was observed to grow inward in the area of the bone defects in

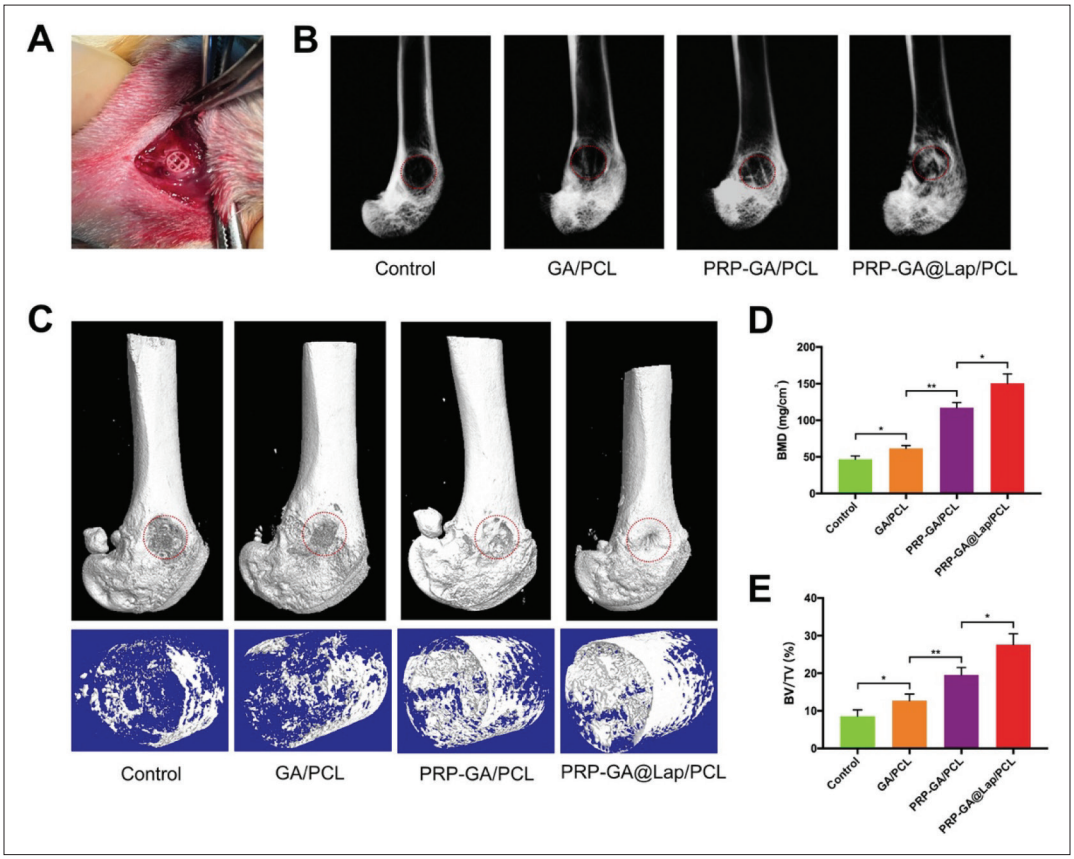

Figure 8. Bone regeneration effects of 3D-printed PRP-GA@Lap/PCL scaffolds *in vivo*. (A) The scaffold was implanted into the area of femoral condylar defect in rats. (B) Representative X-ray images at 1 month after surgery. (C) Representative micro-CT scans and 3D reconstruction images 1 month after surgery. (D, E) Quantification of bone volume to total tissue volume (BV/TV) and bone mineral density (BMD) (n = 6/group). All experiments were replicated three times. *P < 0.05 and **P < 0.01.

all groups (Figure 8C). Quantitative assessment of mineral deposition showed that the BV/TV and BMD at 4 weeks were significantly higher in the PRP-GA/PCL group than in the blank control group and the GA/PCL group but significantly lower than in the PRP-GA@Lap/PCL group (Figure 8D and E). The above results demonstrated that the PRP-GA@Lap/PCL scaffold has a strong bone regenerative capacity *in vivo*.

4. Discussion

Bone defects due to tumor, trauma, inflammation, and infection are collectively a difficult and unsolved problem in orthopedics and a research hotspot because of their high incidence and unsatisfactory prognosis[1,31]. 3D-printed biofunctional scaffolds offer a novel therapeutic approach for the repair and reconstruction of bone defects[32,33]. In the present study, we developed a PRP-GA@Lap composite bioink and demonstrated its excellent biocompatibility and printing performance, in addition to its continuous slow release of multiple growth factors. We demonstrated that this composite hydrogel significantly promoted BMSC osteogenic differentiation, HUVEC tubule formation, and macrophage M2 polarization. This composite bioink was subsequently printed layer-by-layer with PCL using 3D printing technology to construct a bone repair scaffold. Subcutaneous implantation experiments and femoral defect filling repair experiments demonstrated that this bioactive scaffold promotes rapid neovascularization and accelerates bone regeneration *in vivo*.

The encapsulation and delivery of growth factors has great potential for application, but their use in clinical trials has not always shown the expected benefit to patients, with several previous studies reporting significant adverse effects[34-36]. There are multiple causes of these adverse reactions, such as inappropriate delivery methods leading to their release at levels well beyond physiological doses and the high costs associated with these high doses of growth factors.

A great deal of past work has focused on grafting specific growth factors to biomaterials; however, the steps

are cumbersome and the addition of certain chemicals can cause toxic reactions[37]. Instead of selecting a single exogenous growth factor as the main active component of bioink, our study used PRP prepared by centrifugation from whole blood of animals to induce angiogenesis and bone regeneration. PRP, when activated, releases multiple growth factors required for tissue repair in a ratio similar to the normal ratio *in vivo*, allowing for better synergistic effects.

The selection of the optimal concentration of PRP for tissue repair and regeneration applications has also attracted the attention of researchers. Jiang *et al.*[38] integrated 20% PRP into GelMA hydrogel and found that it showed the best effect on proliferation, migration and chondrogenic differentiation of BMSCs, while Zhao *et al.*[39] found that mixed hydrogels containing 5% PRP showed the best effect in promoting fibroblast proliferation and migration. In our study, we mixed GA hydrogel precursor solution with PRP to prepare PRP-based bioinks of different concentration sizes. We found that GA gels containing PRP significantly promoted BMSC proliferation by CCK8 assay, with the 20% PRP-GA and 50% PRP-GA groups showing significantly higher promotion of cell proliferation than the 5% PRP-GA and 10% PRP-GA groups. After 3 and 5 days of culture, there was no significant difference in the proliferation-promoting effect between 20% PRP-GA and 50% PRP-GA (**Figure S2**). This is consistent with the findings of Jiang *et al.*[38]. Based on this, in subsequent experiments, we used the 20% PRP-GA formulation.

Lap is widely used in tissue regeneration due to its excellent drug loading ability. These disk-shaped nanoparticles have negatively charged surfaces and positively charged edges, allowing positively charged growth factors, such as VEGF, to form strong electrostatic bonds with their surfaces, thus exerting a slow release of growth factors[25]. Our study found that although the PRP-GA hydrogel was effective in slowing the release of growth factors, the duration of slow release was not sufficient, and the addition of Lap maintained the release of various growth factors for up to approximately 14 days, which further demonstrates the efficacy of Lap in slowing the release of factors. In addition, Lap material has been reported to significantly promote osteogenic differentiation of BMSCs[40]. Our study found that PRP-GA@Lap and PRP-GA group hydrogels have similar effects in promoting osteogenic differentiation at an early stage. Interestingly, however, by day 14 of culture, we found by Alizarin red staining that the PRP-GA@Lap group produced significantly more calcareous nodules than the other two groups. On the one hand, this may be due to the fact that Lap further prolongs the slow release of growth factors, which enables it to continuously induce osteogenic differentiation of the cells, and on the other hand, several reactive ions released by Lap itself may also play an important role, which is a subject to be further investigated.

The problem of vascularization of bone repair scaffolds has been one of the central challenges in bone defect repair, especially the problem of rapid vascularization[41]. We observed that after 6 h of incubation of HUVECs on the surface of each group, the hydrogels of the two PRP-based groups significantly promoted the formation of HUVEC tubules, demonstrating their potential to promote angiogenesis. Subcutaneous scaffold implantation experiments further validated these findings, but in addition, we observed that the number of vessels in the PRP-GA@Lap/PCL scaffold was significantly greater than that in the PRP-GA/PCL scaffold 1 month after implantation and that the grown-in vessels were more mature. We hypothesize that, in addition to the slow release of pro-angiogenic-related factors, the active ions such as Mg^{2+} and Si^{4+} released by Lap itself may also play an important role, which is a subject for further study.

The transition of macrophages from pro-inflammatory M1 type to later M2 type also plays an important role in tissue repair[42,43]. It has been shown that PRP affects the polarization of macrophages in both *in vivo* and *in vitro* experiments[44]. Our *in vitro* results found that RAW264.7 cells grown on two PRP-containing hydrogels expressed fewer M1-type genes compared to the GA group, while the expression of M2 genes was increased compared to the GA group, suggesting that PRP-GA and PRP-GA@Lap hydrogels promote macrophage polarization toward M2, which is consistent with previous findings[44].

Although our study demonstrates that PRP-based 3D-bioprinted vascularized scaffolds show strong bone regenerative capacity, there are some limitations. On the one hand, we need long-term evaluation studies on large animal models of bone defects; on the other hand, we did not elucidate the specific molecular mechanism of action.

5. Conclusion

In conclusion, we developed a PRP-GA@Lap composite bioink and demonstrated its good osteogenic differentiation and vascularization properties. It was also found to promote macrophage M2 polarization. Furthermore, this bioactive scaffold was shown to promote rapid neovascularization and accelerate bone regeneration *in vivo* through subcutaneous implantation experiments and femoral defect filling repair experiments. This PRP-based bioprinted active scaffold has great clinical translational value.

Acknowledgments

The authors thank the funding support from the General program of NSFC (81972058) and Shanghai Key Clinical Specialty Construction Project - Biomedical Materials (shslczdzk06701), Three-year Action Plan of Shenkang Development Center (SHDC2020CR2019B), Huangpu District Industrial Support Fund (XK2020009), National Key Science and Technology Infrastructure of Translational Medicine (Shanghai) Open Project (TMSZ-2020-207), Shanghai Engineering Research Center of Innovative Orthopedic Instruments and Personalized Medicine (19DZ2250200), Shanghai Science and Technology Commission Yangtze River Delta Science and Technology Innovation Community Project (21002411200), and Technical Standard Project of Shanghai Science and Technology Commission (21DZ2201500).

Conflict of interest

The authors declare no conflicts of interest.

Author contributions

Conceptualization: Bojun Cao, Yongqiang Hao
Investigation: Bojun Cao, Jieming Lin, Jia Tan, Jiaxin Li, Zhaoyang Ran, Liang Deng
Methodology: Yongqiang Hao, Jieming Lin
Supervision: Yongqiang Hao
Writing – original draft: Bojun Cao
Writing – review & editing: Bojun Cao, Yongqiang Hao

The manuscript is approved by all authors for publication.

Ethics approval and consent to participate

All protocols involving experimental animals were approved by the Animal Welfare Ethics Committee of the Ninth People's Hospital Affiliated to Shanghai Jiaotong University School of Medicine (SH9H-2019-A717-1).

Consent for publication

Not applicable.

Availability of data

Data will be made available on request.

References

1. Armiento AR, Hatt LP, Rosenberg GS, *et al.*, 2020, Functional biomaterials for bone regeneration: A lesson in complex biology. *Adv Funct Mater*, 30(44):1909874.

   https://doi.org/10.1002/adfm.201909874

2. Zhang YB, Liu XC, Zeng LD, *et al.*, 2019, Polymer fiber scaffolds for bone and cartilage tissue engineering. *Adv Funct Mater*, 29(36):1903279.

   https://doi.org/10.1002/adfm.201903279

3. Zheng CC, Attarilar S, Li K, *et al.*, 2021, 3D-printed HA15-loaded beta-tricalcium phosphate/poly (lactic-co-glycolic acid) bone tissue scaffold promotes bone regeneration in rabbit radial defects. *Int J Bioprint*, 7(1):100–111.

   https://doi.org/10.18063/ijb.v7i1.317

4. Li Y, Xie KG, Wang C, *et al.*, 2021, 3D printing of tricalcium phosphate/poly lactic-co-glycolic acid. Scaffolds loaded with carfilzomib for treating critical-sized rabbit radial bone defects. *Int J Bioprint*, 7(4):99–111.

   https://doi.org/10.18063/ijb.v7i4.405

5. Lin ZF, Wu MM, He HM, *et al.*, 2019, 3D printing of mechanically stable calcium-free alginate-based scaffolds with tunable surface charge to enable cell adhesion and facile biofunctionalization. *Adv Funct Mater*, 29(9):1808439.

   https://doi.org/10.1002/adfm.201808439

6. Groll J, Burdick JA, Cho DW, *et al.*, 2019, A definition of bioinks and their distinction from biomaterial inks. *Biofabrication*, 11(1):013001.

   https://doi.org/10.1088/1758-5090/aaec52

7. Zhang S, Chen J, Yu Y, *et al.*, 2019, Accelerated bone regenerative efficiency by regulating sequential release of BMP-2 and VEGF and synergism with sulfated chitosan. *ACS Biomater Sci Eng*, 5(4):1944–1955.

   https://doi.org/10.1021/acsbiomaterials.8b01490

8. Kempen DH, Lu L, Heijink A, *et al.*, 2009, Effect of local sequential VEGF and BMP-2 delivery on ectopic and orthotopic bone regeneration. *Biomaterials*, 30(14): 2816–2825.

   https://doi.org/10.1016/j.biomaterials.2009.01.031

9. Geuze RE, Theyse LF, Kempen DH, *et al.*, 2012, A differential effect of bone morphogenetic protein-2 and vascular endothelial growth factor release timing on osteogenesis at ectopic and orthotopic sites in a large-animal model. *Tissue Eng Part A*, 18(19-20):2052–2062.

   https://doi.org/10.1089/ten.TEA.2011.0560

10. Wei S, Xu P, Yao Z, *et al.*, 2021, A composite hydrogel with co-delivery of antimicrobial peptides and platelet-rich plasma to enhance healing of infected wounds in diabetes. *Acta Biomater*, 124:205–218.

    https://doi.org/10.1016/j.actbio.2021.01.046

11. Singh M, Nanda HS, Lee JYH, *et al.*, 2020, Photocurable platelet rich plasma bioadhesives. *Acta Biomater*, 117: 133–141.

    https://doi.org/10.1016/j.actbio.2020.09.030

12. Iyer SR, Scheiber AL, Yarowsky P, *et al.*, 2020, Exosomes isolated from platelet-rich plasma and mesenchymal stem cells promote recovery of function after muscle injury. *Am J Sports Med*, 48(9):2277–2286.

https://doi.org/10.1177/0363546520926462

13. Uludag H, D'Augusta D, Palmer R, *et al.*, 1999, Characterization of rhBMP-2 pharmacokinetics implanted with biomaterial carriers in the rat ectopic model. *J Biomed Mater Res*, 46(2):193–202.

https://doi.org/10.1002/(sici)1097-4636(199908)46:2<193::aid-jbm8>3.0.co;2-1

14. Bouletreau PJ, Warren SM, Spector JA, *et al.*, 2002, Hypoxia and VEGF up-regulate BMP-2 mRNA and protein expression in microvascular endothelial cells: Implications for fracture healing. *Plast Reconstr Surg*, 109(7):2384–2397.

https://doi.org/10.1097/00006534-200206000-00033

15. Pufe T, Wildemann B, Petersen W, *et al.*, 2002, Quantitative measurement of the splice variants 120 and 164 of the angiogenic peptide vascular endothelial growth factor in the time flow of fracture healing: A study in the rat. *Cell Tissue Res*, 309(3):387–392.

https://doi.org/10.1007/s00441-002-0605-0

16. Uchida S, Sakai A, Kudo H, *et al.*, 2003, Vascular endothelial growth factor is expressed along with its receptors during the healing process of bone and bone marrow after drill-hole injury in rats. *Bone*, 32(5):491–501.

https://doi.org/10.1016/s8756-3282(03)00053-x

17. Schär MO, Diaz-Romero J, Kohl S, *et al.*, 2015, Platelet-rich concentrates differentially release growth factors and induce cell migration in vitro. *Clin Orthop Relat Res*, 473(5):1635–1643.

https://doi.org/10.1007/s11999-015-4192-2

18. Dohan Ehrenfest DM, Rasmusson L, Albrektsson T, 2009, Classification of platelet concentrates: From pure platelet-rich plasma (P-PRP) to leucocyte- and platelet-rich fibrin (L-PRF). *Trends Biotechnol*, 27(3):158–167.

https://doi.org/10.1016/j.tibtech.2008.11.009

19. Chuah YJ, Peck Y, Lau JE, *et al.*, 2017, Hydrogel based cartilaginous tissue regeneration: Recent insights and technologies. *Biomater Sci*, 5(4):613–631.

https://doi.org/10.1039/c6bm00863a

20. Yue K, Trujillo-de Santiago G, Alvarez MM, *et al.*, 2015, Synthesis, properties, and biomedical applications of gelatin methacryloyl (GelMA) hydrogels. *Biomaterials*, 73:254–271.

https://doi.org/10.1016/j.biomaterials.2015.08.045

21. Chu C, Deng J, Sun X, *et al.*, 2017, Collagen membrane and immune response in guided bone regeneration: Recent progress and perspectives. *Tissue Eng Part B Rev*, 23(5):421–435.

https://doi.org/10.1089/ten.TEB.2016.0463

22. Niu X, Ferracci G, Lin M, *et al.*, 2021, Highly substituted decoupled gelatin methacrylamide free of hydrolabile methacrylate impurities: An optimum choice for long-term stability and cytocompatibility. *Int J Biol Macromol*, 167:479–490.

https://doi.org/10.1016/j.ijbiomac.2020.11.187

23. Krishna KV, Ménard-Moyon C, Verma S, *et al.*, 2013, Graphene-based nanomaterials for nanobiotechnology and biomedical applications. *Nanomedicine (Lond)*, 8(10):1669–1688.

https://doi.org/10.2217/nnm.13.140

24. Waters R, Pacelli S, Maloney R, *et al.*, 2016, Stem cell secretome-rich nanoclay hydrogel: A dual action therapy for cardiovascular regeneration. *Nanoscale*, 8(14):7371–7376.

https://doi.org/10.1039/c5nr07806g

25. Ding X, Gao J, Wang Z, *et al.*, 2016, A shear-thinning hydrogel that extends in vivo bioactivity of FGF2. *Biomaterials*, 111:80–89.

https://doi.org/10.1016/j.biomaterials.2016.09.026

26. Zhang Y, Xu J, Ruan YC, *et al.*, 2016, Implant-derived magnesium induces local neuronal production of CGRP to improve bone-fracture healing in rats. *Nat Med*, 22(10):1160–1169.

https://doi.org/10.1038/nm.4162

27. Lee CS, Hwang HS, Kim S, *et al.*, 2020, Inspired by nature: Facile design of nanoclay-organic hydrogel bone sealant with multifunctional properties for robust bone regeneration. *Adv Funct Mater*, 30(43):2003717.

https://doi.org/10.1002/adfm.202003717

28. Cao BJ, Wang XW, Zhu L, *et al.*, 2019, MicroRNA-146a sponge therapy suppresses neointimal formation in rat vein grafts. *IUBMB Life*, 71(1):125–133.

https://doi.org/10.1002/iub.1946

29. Cao BJ, Wang XW, Zhu L, *et al.*, 2019, Dedicator of cytokinesis 2 silencing therapy inhibits neointima formation and improves blood flow in rat vein grafts. *J Mol Cell Cardiol*, 128:134–144.

https://doi.org/10.1016/j.yjmcc.2019.01.030

30. Liu X, Yang Y, Niu X, *et al.*, 2017, An in situ photocrosslinkable platelet rich plasma—Complexed hydrogel glue with growth factor controlled release ability to promote cartilage defect repair. *Acta Biomater*, 62:179–187.

https://doi.org/10.1016/j.actbio.2017.05.023

31. Daskalakis E, Liu FY, Huang BY, *et al.*, 2021, Investigating the influence of architecture and material composition of 3D printed anatomical design scaffolds for large bone defects. *Int J Bioprint*, 7(2):43–52.

https://doi.org/10.18063/ijb.v7i2.268

32. Shao H, Liu A, Ke X, *et al.*, 2017, 3D robocasting magnesium-doped wollastonite/TCP bioceramic scaffolds with improved bone regeneration capacity in critical sized calvarial defects. *J Mater Chem B*, 5(16):2941–2951.

https://doi.org/10.1039/c7tb00217c

33. Matai I, Kaur G, Seyedsalehi A, *et al.*, 2020, Progress in 3D bioprinting technology for tissue/organ regenerative engineering. *Biomaterials*, 226:119536.

https://doi.org/10.1016/j.biomaterials.2019.119536

34. Epstein NE, 2013, Complications due to the use of BMP/INFUSE in spine surgery: The evidence continues to mount. *Surg Neurol Int*, 4(Suppl 5):S343–S352.

https://doi.org/10.4103/2152-7806.114813

35. Shields LB, Raque GH, Glassman SD, *et al.*, 2006, Adverse effects associated with high-dose recombinant human bone morphogenetic protein-2 use in anterior cervical spine fusion. *Spine (Phila Pa 1976)*, 31(5):542–547.

https://doi.org/10.1097/01.brs.0000201424.27509.72

36. Lee K, Silva EA, Mooney DJ, 2011, Growth factor delivery-based tissue engineering: General approaches and a review of recent developments. *J R Soc Interface*, 8(55):153–170.

https://doi.org/10.1098/rsif.2010.0223

37. Liu KT, Zhao M, Li Y, *et al.*, 2022, VEGF loaded porcine decellularized adipose tissue derived hydrogel could enhance angiogenesis in vitro and in vivo. *J Biomater Sci Poly Ed*, 33(5):569–589.

https://doi.org/10.1080/09205063.2021.2002235

38. Jiang GY, Li SH, Yu K, *et al.*, 2021, A 3D-printed PRP-GelMA hydrogel promotes osteochondral regeneration through M2 macrophage polarization in a rabbit model. *Acta Biomater*, 128:150–162.

https://doi.org/10.1016/j.actbio.2021.04.010

39. Zhao M, Wang J, Zhang JX, *et al.*, 2022, Functionalizing multi-component bioink with platelet-rich plasma for customized in-situ bilayer bioprinting for wound healing. *Mater Today Bio*, 16:100334.

https://doi.org/10.1016/j.mtbio.2022.100334

40. Gaharwar AK, Mihaila SM, Swami A, *et al.*, 2013, Bioactive silicate nanoplatelets for osteogenic differentiation of human mesenchymal stem cells. *Adv Mater*, 25(24):3329–3336.

https://doi.org/10.1002/adma.201300584

41. Stegen S, van Gastel N, Carmeliet G, 2015, Bringing new life to damaged bone: The importance of angiogenesis in bone repair and regeneration. *Bone*, 70:19–27.

https://doi.org/10.1016/j.bone.2014.09.017

42. Klopfleisch R, Jung F, 2017, The pathology of the foreign body reaction against biomaterials. *J Biomed Mater Res A*, 105(3):927–940.

https://doi.org/10.1002/jbm.a.35958

43. Brown BN, Badylak SF, 2013, Expanded applications, shifting paradigms and an improved understanding of host-biomaterial interactions. *Acta Biomater*, 9(2):4948–4955.

https://doi.org/10.1016/j.actbio.2012.10.025

44. Papait A, Cancedda R, Mastrogiacomo M, *et al.*, 2018, Allogeneic platelet-rich plasma affects monocyte differentiation to dendritic cells causing an anti-inflammatory microenvironment, putatively fostering wound healing. *J Tissue Eng Regen Med*, 12(1):30–43.

https://doi.org/10.1002/term.2361